

---

---

# Quantitative Radiomics Features in Diffuse Large B-Cell Lymphoma: Does Segmentation Method Matter?

Jakoba J. Eertink<sup>1</sup>, Elisabeth A.G. Pfaehler<sup>2</sup>, Sanne E. Wiegers<sup>1</sup>, Tim van de Brug<sup>3</sup>, Pieternella J. Lugtenburg<sup>4</sup>, Otto S. Hoekstra<sup>5</sup>, Josée M. Zijlstra<sup>1</sup>, Henrica C.W. de Vet<sup>3</sup>, and Ronald Boellaard<sup>5</sup>

<sup>1</sup>Department of Hematology, Amsterdam UMC, Vrije Universiteit Amsterdam, Cancer Center Amsterdam, Amsterdam, The Netherlands; <sup>2</sup>Department of Nuclear Medicine, University Hospital Augsburg, Augsburg, Germany; <sup>3</sup>Department of Epidemiology and Data Science, Amsterdam UMC, Vrije Universiteit Amsterdam, Amsterdam Public Health Research Institute, Amsterdam, The Netherlands; <sup>4</sup>Department of Hematology, Erasmus MC Cancer Institute, University Medical Center Rotterdam, Rotterdam, The Netherlands; and <sup>5</sup>Department of Radiology and Nuclear Medicine, Amsterdam UMC, Vrije Universiteit Amsterdam, Cancer Center Amsterdam, Amsterdam, The Netherlands

Radiomics features may predict outcome in diffuse large B-cell lymphoma (DLBCL). Currently, multiple segmentation methods are used to calculate metabolic tumor volume (MTV). We assessed the influence of segmentation method on the discriminative power of radiomics features in DLBCL at the patient level and for the largest lesion. **Methods:** Fifty baseline <sup>18</sup>F-FDG PET/CT scans of DLBCL patients with progression or relapse within 2 years after diagnosis were matched on uptake time and reconstruction method with 50 baseline PET/CT scans of DLBCL patients without progression. Scans were analyzed using 6 semiautomatic segmentation methods (SUV threshold of 4.0 [SUV4.0], SUV threshold of 2.5, 41% of SUV<sub>max</sub>, 50% of SUV<sub>peak</sub>, a majority vote segmenting voxels detected by  $\geq 2$  methods, and a majority vote segmenting voxels detected by  $\geq 3$  methods). On the basis of these segmentations, 490 radiomics features were extracted at the patient level, and 486 features were extracted for the largest lesion. To quantify the agreement between features extracted from different segmentation methods, the intraclass correlation (ICC) agreement was calculated for each method compared with SUV4.0. The feature space was reduced by deleting features that had high Pearson correlations ( $\geq 0.7$ ) with the previously established predictors MTV or SUV<sub>peak</sub>. Model performance was assessed using stratified repeated cross validation with 5 folds and 2,000 repeats, yielding the mean receiver-operating-characteristics curve integral for all segmentation methods using logistic regression with backward feature selection. **Results:** The percentage of features yielding an ICC of at least 0.75, compared with the SUV4.0 segmentation, was lowest for 50% of SUV<sub>peak</sub> both at the patient level and for the largest lesion, with 77.3% and 66.7% of the features yielding an ICC of at least 0.75, respectively. Features did not correlate strongly with MTV, with at least 435 features at the patient level and 409 features for the largest lesion for all segmentation methods having a correlation coefficient of less than 0.7. Features correlated strongly with SUV<sub>peak</sub> (at least 190 at patient level and 134 for the largest lesion were uncorrelated to SUV<sub>peak</sub>, respectively). Receiver-operating-characteristics curve integrals ranged between  $0.69 \pm 0.11$  and  $0.84 \pm 0.09$  at the patient level and between  $0.69 \pm 0.11$  and  $0.73 \pm 0.10$  at the lesion level. **Conclusion:** Even though there are differences in the actual radiomics feature values derived and selected features among segmentation methods, there is no

substantial difference in the discriminative power of radiomics features among segmentation methods.

**Key Words:** diffuse large B-cell lymphoma; segmentation methods; radiomics; <sup>18</sup>F-FDG PET/CT

**J Nucl Med 2022; 63:389–395**

DOI: 10.2967/jnumed.121.262117

**D**iffuse large B-cell lymphoma (DLBCL) is the most common subtype of non-Hodgkin lymphoma. To improve the outcome of patients with DLBCL, early identification of patients at risk of treatment failure is of the utmost importance, as 25%–40% of patients experience relapse or progression in the first years after diagnosis (1). Recent data suggest that baseline radiomics features are promising biomarkers to predict treatment outcome in DLBCL (2–4), as they can predict outcome beyond metabolic tumor volume (MTV) and the international prognostic index (5).

Radiomics features can be calculated from the baseline <sup>18</sup>F-FDG PET/CT scans and capture detailed and quantitative information on, for example, texture, intensity, and shape of lesions. Currently, radiomics analyses in lymphoma are based on predefined tumor segmentations. Segmentations are usually performed using absolute SUV thresholds (6) or percentages of SUV<sub>max</sub> or SUV<sub>peak</sub> (2,7). For the calculation of radiomics features, some studies use the hottest lesion (4), whereas others use the largest lesion (3,8) or tumor segmentations at the patient level (2,9). The largest lesion and MTV at the patient level had the highest predictive value (9). Therefore, in this study we concentrated on the largest lesion and radiomics features extracted from tumor segmentations at the patient level.

One of the main problems with generating a multitude of features is the high false-detection rate caused by multiple testing. Moreover, several features may represent similar characteristics that are often highly correlated and therefore redundant (10). Redundant features may induce a correlation bias (11), and models become difficult to interpret (12).

Therefore, reducing the feature space to a degree feasible for clinical use without losing important information is essential. One method to reduce feature space is hierarchical clustering, based on correlation analysis or distance metrics (13).

Previous DLBCL studies showed that MTV measured with different segmentation methods, albeit at different cutoffs, showed

---

Received Feb. 12, 2021; revision accepted Jun. 3, 2021.  
For correspondence or reprints, contact Ronald Boellaard (r.boellaard@amsterdamumc.nl).  
Published online Jul. 16, 2021.  
COPYRIGHT © 2022 by the Society of Nuclear Medicine and Molecular Imaging.

comparable discriminative power to predict survival (6,7). However, it is unclear to what extent the discriminative power of other radiomics features is affected by the method used to segment the lesions. Therefore, our main objective was to assess the effects of applying 6 frequently used segmentation methods on the discriminative power for 2-year time to progression of baseline PET/CT radiomics features in DLBCL both at the patient level and for the largest lesion.

## MATERIALS AND METHODS

### Study Population

For this case-control study, 100 patients with newly diagnosed DLBCL from the HOVON-84 study (Haemato Oncology Foundation for Adults in the Netherlands; European Union Drug Regulating Authorities Clinical Trials Database identifier 2006-005174-42) with baseline PET/CT scans available were included. Fifty patients with progressive disease or relapse within 2 years after diagnosis were matched on scan interval and reconstruction method (European Association of Nuclear Medicine Research GmbH [EARL]/non-EARL) (14) with 50 patients without progression. For this analysis, we combined R-CHOP14 (14-d cycles of rituximab plus cyclophosphamide, doxorubicin, vincristine, and prednisone) and RR-CHOP14 (rituximab-intensified R-CHOP-14), because outcomes were similar between treatment arms (15). The HOVON-84 study was approved by the institutional review board, and all participants gave informed consent.

### Quantitative Analysis

Quantitative PET/CT analysis was performed using the quantitative oncology molecular analysis suite (ACCURATE) (16). To match quality criteria, PET and low-dose CT scans should be complete, and liver  $SUV_{mean}$  and plasma glucose should be within the ranges suggested by the European Association of Nuclear Medicine guidelines (14). If liver  $SUV_{mean}$  was outside the suggested ranges but total image activity was between 50% and 80% of the injected activity, the scans were still included. All scans were reviewed by nuclear medicine physicians, and delineations were performed under their supervision. The following frequently used semiautomatic segmentation methods were applied to delineate lesions: an SUV threshold of 2.5, an SUV threshold of 4.0 ( $SUV_{4.0}$ ). 50% of  $SUV_{peak}$  (17), 41% of  $SUV_{max}$ , a majority vote segmenting voxels detected by at least 2 methods, and a majority vote segmenting voxels detected by at least 3 methods (supplemental materials; available at <http://jnm.snmjournals.org>).

Lesions were delineated with a fully automated preselection of lesions with a volume threshold of at least  $3\text{ cm}^3$ . Lymphoma lesions smaller than  $3\text{ cm}^3$  were added by observer selection, and nontumor regions were deleted with single mouse-clicks for all 6 segmentation methods (18). Lesions for which automatic segmentation was successful were added to the patient-level volume of interest. If lesion selection resulted in flooding (i.e., selection of large parts of nontumor regions, such as liver, spleen, or skeleton), the lesion was not added. Adjacent nontumor  $^{18}\text{F}$ -FDG-avid regions (e.g., bladder or kidney) were manually removed. For the fixed  $SUV_{4.0}$  method, we also generated segmentations with a volume threshold of at least  $3\text{ cm}^3$ . Two observers selected the method with the highest visual agreement (best method) for each patient, resolving initial discrepancies in consensus meetings.

### Feature Extraction

Four hundred eighty radiomics features (texture [ $n = 408$ ], morphology [ $n = 22$ ], intensity-based statistics [ $n = 18$ ], intensity histogram [ $n = 24$ ], intensity-volume histogram [ $n = 6$ ], and local intensity [ $n = 2$ ]) and 6 conventional PET uptake metrics before rebinning were extracted for both the patient level and the largest lesion for each segmentation method. The patient-level volume of interest included all segmented lesions and was generated by assigning all voxels within the

individual lesions to one and all voxels outside any of the segmented individual lesions to zero. At the patient level, 4 additional dissemination features were calculated. All image-processing and feature calculations were performed using RaCat software (19), which complies with the imaging biomarker standardization initiative criteria (20). Details on feature calculation are presented in the supplemental materials.

### Statistical Analysis

All statistical analyses were performed for radiomics features at the patient level and for the largest lesion using R (version 4.0.3). The paired Student *t* test was used to compare the MTV and  $SUV_{peak}$  of all segmentation methods with the best segmentation. On the basis of recent studies, the  $SUV_{4.0}$  segmentation was chosen as a reference (7,18). First, if the distribution of the radiomics feature values had skewness greater than 0.5 for the  $SUV_{4.0}$  segmentation method, they were log-transformed for all segmentations using the natural logarithm. The agreement between radiomics features extracted from different segmentations was quantified by calculating the intraclass correlation (ICC) compared with the  $SUV_{4.0}$  segmentation. ICCs were categorized as having reliability that was poor ( $<0.5$ ), moderate (0.5–0.74), good (0.75–0.89), or excellent ( $\geq 0.90$ ) (21). Two texture features at the patient level and 3 texture features at the lesion level did not show any variation and were therefore excluded.

MTV and  $SUV_{peak}$  have been shown to be predictive in DLBCL (9). To avoid overfitting and to remove redundancy, the feature space was reduced by deleting features that correlated strongly with either MTV or  $SUV_{peak}$ . The Pearson correlation coefficient between MTV and other radiomics features, and between  $SUV_{peak}$  and other radiomics features, was calculated for each segmentation method. A correlation was considered high if the Pearson correlation coefficient was at least 0.7 (22).

For each segmentation method, the mutual correlations between features that did not correlate with MTV and  $SUV_{peak}$  were calculated using Pearson correlation. For clusters of features with high mutual correlations, as identified with hierarchical clustering using Euclidian distance as a distance measure, the feature with the lowest correlation to MTV or  $SUV_{peak}$  was preserved.

Discriminative power (progression vs. nonprogression) was assessed using logistic regression with backward feature selection based on the Akaike information criteria (23). We included all independent features, MTV, and  $SUV_{peak}$  for all segmentations. Stratified repeated cross validation with 5 folds and 2,000 repeats was applied, yielding the mean receiver-operating-characteristic curve integral (CV-AUC) and the SD of AUCs between repeats. Comparing CV-AUCs is a known difficulty because of the inherent dependency of train-test iterations and complex relations between the trained models (24). Currently, there is no valid statistical approach to compare CV-AUCs.

As a sensitivity evaluation, all analyses were repeated for features that were reliable, repeatable, and reproducible in a multicenter setting (25).

## RESULTS

Patient characteristics are summarized in Table 1. Sixty-four scans were semiautomatically analyzed and adapted with single mouse-clicks only. Thirty-six scans required manual editing because tumor and nontumor regions were adjacent.  $SUV_{4.0}$  was selected most frequently as the best method for both the patient level and the lesion level (49% and 64%, respectively).

### MTV Analysis

The method using an SUV threshold of 2.5 resulted in MTV flooding for 44 patients, leading to exclusion of this method for further analysis. At the patient and lesion levels, MTV was highest for the segmentation using a majority vote segmenting voxels

**TABLE 1**  
Characteristics of Included Patients

Characteristic	Events	Nonevents
<b>Age</b>		
Median (y)	64 (IQR, 61–71)	68 (IQR, 63–74)
≤60 y	11	11
>60 y	39	39
<b>Sex</b>		
Male	28	26
Female	22	24
<b>Ann Arbor stage</b>		
2	3	6
3	9	13
4	38	31
<b>Lactate dehydrogenase</b>		
Normal	8	19
>normal	42	31
<b>Extranodal localizations</b>		
≤1	21	28
>1	29	22
<b>Performance status</b>		
0	16	29
1	25	13
2	9	8
<b>International prognostic index</b>		
Low	3	5
Low-intermediate	2	14
High-intermediate	25	18
High	20	13

IQR = interquartile range.

detected by at least 2 methods and was lowest for the method using 50% of  $SUV_{peak}$  (Table 2). Using the best visual segmentation as a reference, MTV was significantly higher for the segmentation using a majority vote segmenting voxels detected by at least 2 methods and was significantly lower using all other segmentation methods (all  $P < 0.05$ ; Table 2; Fig. 1).  $SUV_{peak}$  was comparable among segmentation methods (all  $P > 0.05$ ).

#### Patient Level

Radiomics features based on a SUV4.0 preselection with a 3-cm<sup>3</sup> volume threshold resembled the features of the SUV4.0 segmentation most, with excellent reliability for 414 features (84.8%), followed by the best segmentation. For the segmentation using 50% of  $SUV_{peak}$ , similarity was lowest, with only 218 features (44.7%) having excellent reliability (Fig. 2; Supplemental Table 1).

For all segmentation methods, at least 435 features (89.3%) did not correlate strongly with MTV (Table 3), of which 433 (88.9%) did not correlate strongly with MTV for any segmentation method. At least 190 features (38.9%) did not correlate strongly with  $SUV_{peak}$ , of which 175 (35.9%) did not correlate strongly with  $SUV_{peak}$  for any segmentation. One hundred ninety-seven features (40.5%) did not correlate with MTV and  $SUV_{peak}$  for at least 1 method, of which 125 (25.7%) correlated neither with MTV nor with  $SUV_{peak}$  for any segmentation method. For each segmentation method, at least 25 features (5.1%) did not show high mutual correlations and did not correlate with MTV or  $SUV_{peak}$ . After backward feature selection, the SUV4.0 segmentation method yielded a CV-AUC of  $0.74 \pm 0.10$ ; 41% of  $SUV_{max}$  had the highest CV-AUC ( $0.84 \pm 0.09$ ), the visually best segmentation method had the lowest CV-AUC ( $0.69 \pm 0.11$ ). Selected features after backward selection differed among segmentation methods and varied between 4 and 20 features (Table 3; Supplemental Table 2). For all segmentation methods, the morphologic feature “center of mass shift” and the texture feature “first measure of information correlation” were retained in the linear regression model.

#### Largest Lesion

Radiomics features of the segmentation using a majority vote segmenting voxels detected by at least 2 methods resembled those

**TABLE 2**  
 $SUV_{peak}$  and MTV per Segmentation Method

Parameter	$SUV_{peak}$	MTV patient level	MTV largest lesion
SUV4.0	17.1 (12.8–22.0)	552.7 (310.3–1,117.2)	353.5 (145.3–854.4)
SUV4.0 ( $\geq 3$ cm <sup>3</sup> )	17.2 (12.8–22.3)	534.8 (295.4–1,116.4)	353.5 (145.3–854.4)
A50P	16.8 (12.5–22.0)	463.5 (210.2–1,164.0)	264.6 (75.9–658.1)
41%max	16.8 (12.5–22.0)	492.0 (230.3–1,203.5)	295.3 (112.6–741.8)
MV2	16.8 (12.8–22.0)	726.2 (374.5–1,299.9)	445.1 (188.0–1041.6)
MV3	16.8 (12.5–22.3)	502.5 (235.5–1,155.0)	280.2 (98.9–693.9)
Best	16.6 (12.4–21.9)	653.2 (350.5–1,283.8)	445.1 (172.6–935.5)

A50P = 50% of  $SUV_{peak}$ ; 41%max = 41% of  $SUV_{max}$ ; MV2 = majority vote segmenting voxels detected by  $\geq 2$  methods; MV3 = majority vote segmenting voxels detected by  $\geq 3$  methods.

Data are median followed by interquartile range.

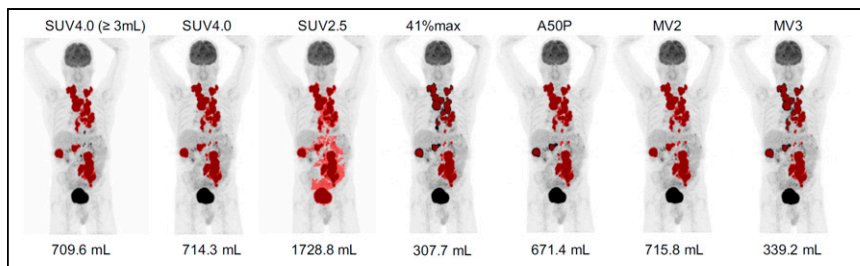


**FIGURE 1.** Maximum-intensity PET projections of patient with lesion segmentations indicated in red for all applied methods using SUV scale of 0–10. 41%max = 41% of  $SUV_{max}$ ; A50P = 50% of  $SUV_{peak}$ ; MV2 = majority vote segmenting voxels detected by  $\geq 2$  methods; MV3 = majority vote segmenting voxels detected by  $\geq 3$  methods; SUV2.5 = SUV threshold of 2.5.

of the SUV4.0 method most, with excellent reliability for 389 features (80.5%). For the segmentation using 50% of  $SUV_{peak}$ , similarity was lowest, at only 83 features (17.2%) with excellent reliability (Fig. 3; Supplemental Table 3).

For all segmentations, at least 409 features (84.9%) did not correlate strongly with MTV (Table 4), of which 404 (83.8%) did not correlate strongly with MTV for any segmentation method. At least 134 features (27.8%) did not correlate strongly with  $SUV_{peak}$ , of which 130 features (27.0%) did not correlate strongly with  $SUV_{peak}$  for any segmentation. One hundred forty-nine (31.0%) features did not correlate with MTV or  $SUV_{peak}$  for at least 1 method, of which 61 features (12.7%) correlated neither with MTV nor with  $SUV_{peak}$  for any segmentation method. For each segmentation method, at least 19 features (4.0%) did not show high mutual correlations and did not correlate with MTV or  $SUV_{peak}$ . After backward feature selection, SUV4.0 had the highest CV-AUC ( $0.73 \pm 0.10$ ), whereas a majority vote segmenting voxels detected by at least 3 methods and the best segmentation method had the lowest CV-AUC ( $0.69 \pm 0.11$ ). Selected features after backward selection differed among segmentation methods and varied between 5 and 11 features (Table 4; Supplemental Table 4). For all segmentation methods, the texture feature “first measure of information correlation” was retained in the linear regression model, and the intensity histogram feature “minimum

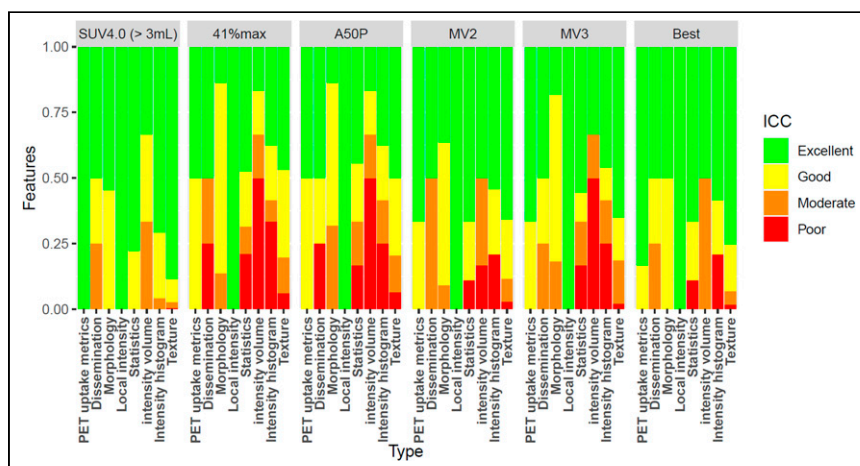


**FIGURE 2.** Percentage of radiomics features yielding excellent, good, moderate, or poor ICC agreement between SUV4.0 segmentation and the other methods at the patient level. 41%max = 41% of  $SUV_{max}$ ; A50P = 50% of  $SUV_{peak}$ ; MV2 = majority vote segmenting voxels detected by  $\geq 2$  methods; MV3 = majority vote segmenting voxels detected by  $\geq 3$  methods.

histogram gradient” was retained in all models except for the SUV4.0 segmentation method.

When starting from a selection with reliable, repeatable, and reproducible features, similar results were found both at the patient level and for the largest lesion (Table 3; Table 4).

## DISCUSSION

This study showed that the discriminative power is largely independent of segmentation method. However, there are large differences in radiomics feature values derived using different segmentation methods, as shown by ICC agreement values.

Both MTV and  $SUV_{peak}$  have been shown to be predictive in DLBCL (9). Our study showed that most radiomics features are independent of MTV for both the patient level and the largest lesion. Hatt et al. (26) showed that textural features, which comprise more than 80% of our radiomics features, already provide clinical complementary information in addition to MTV in lesions larger than  $10 \text{ cm}^3$ , with an increasing complementary prognostic value for larger MTVs, disputing the threshold for texture features of  $45 \text{ cm}^3$  (27). With only 4 patients with MTVs smaller than  $10 \text{ cm}^3$  for the largest lesion, and 1 patient with an MTV smaller than  $10 \text{ cm}^3$  at the patient level, it is to be expected that most features are independent of MTV. However, many features correlated with  $SUV_{peak}$ , in which case they are redundant.

Currently, there is no consensus on the best segmentation method for delineating lesions in DLBCL  $^{18}\text{F}$ -FDG PET/CT studies. Therefore, it is essential to study the sensitivity of radiomics features in relation to segmentation method. In several solid cancers, radiomics features, especially morphologic and texture features, are influenced by the delineation method (28–31). The number of extracted features in these studies varied widely, between 9 and 480. We extend these findings by showing that for the largest lesion in DLBCL, up to 31% of the texture features, and 68% of the morphologic features, were highly sensitive to the segmentation method, as shown by the reliability of features compared with SUV4.0 segmentation. DLBCL lesions usually are large, heterogeneous, and bulky. Larger lesions are known to exhibit higher hypoxia, necrosis, or anatomic and physiologic complexity—characteristics that logically translate to higher complexity in the spatial  $^{18}\text{F}$ -FDG distribution and hence sensitivity to segmentation method, leading to lower reliability of features among applied methods. Furthermore, as variations in segmentation methods have a strong effect on the outer contour of the segmentation, thus influencing the shape of the segmentation, a high sensitivity to segmentation methods for morphologic features could be expected. Because of the higher MTV, the radiomics features at the patient level were less

**TABLE 3**

Number of Independent Features per Segmentation Method, Number of Included Features, and Predictive Value at Patient Level for All Extracted Features ( $n = 488$ ) and All Reliable, Repeatable, and Reproducible Features ( $n = 103$ )

No of features	Parameter	Independent of MTV	Independent of SUV <sub>peak</sub>	Independent of MTV and SUV <sub>peak</sub>	Independent of MTV and SUV <sub>peak</sub> and uncorrelated	No. of features in linear regression	CV-AUC ( $\pm$ SD)
488	SUV4.0	445	211	172	25	12	0.74 $\pm$ 0.10
	SUV4.0 ( $\geq 3$ cm <sup>3</sup> )	443	212	170	25	4	0.74 $\pm$ 0.10
	41%max	435	198	145	27	11	0.84 $\pm$ 0.09
	A50P	441	204	157	32	20	0.78 $\pm$ 0.10
	MV2	444	199	155	26	5	0.79 $\pm$ 0.09
	MV3	441	203	156	29	18	0.80 $\pm$ 0.09
	Best	445	190	147	25	12	0.69 $\pm$ 0.11
103	SUV4.0	64	63	35	13	3	0.70 $\pm$ 0.11
	SUV4.0 ( $\geq 3$ cm <sup>3</sup> )	61	63	32	12	6	0.70 $\pm$ 0.11
	41%max	54	63	24	10	4	0.75 $\pm$ 0.10
	A50P	58	65	30	10	3	0.63 $\pm$ 0.11
	MV2	61	66	34	11	8	0.74 $\pm$ 0.10
	MV3	58	65	30	9	4	0.73 $\pm$ 0.10
	Best	62	67	36	11	7	0.69 $\pm$ 0.11

41%max = 41% of SUV<sub>max</sub>; A50P = 50% of SUV<sub>peak</sub>; MV2 = majority vote segmenting voxels detected by  $\geq 2$  methods; MV3 = majority vote segmenting voxels detected by  $\geq 3$  methods.

influenced by segmentation method, with up to 20% of the texture features, and 32% of the morphology features, being sensitive to segmentation method. Because of the low similarity of some of the features between segmentations, it is not advisable to use regression coefficients from other studies that applied other segmentation methods.

However, even though values are not interchangeable, in our study the discriminative power at the lesion and patient levels was comparable among segmentations. Contrary to what we expected, choosing the segmentation method that visually best selected the tumors did not result in a higher CV-AUC. These results are in line with previous studies exploring the predictive value of radiomics

features using different segmentations for other cancer types. None of these studies found significant differences in predicting outcome (28,32), metastasis, or lymph node invasion (30) using different segmentation methods. However, ICC agreement values, correlations with MTV, correlations with SUV<sub>peak</sub>, and mutual correlations differed among segmentation methods, resulting in different preselections of features for the logistic regression model. Even though discriminative power is comparable, different features are predictive of outcome when applying different segmentation methods.

When using only previously defined reliable, repeatable, and reproducible features, discriminative power was slightly lower for all segmentation methods. However, the CIs of CV-AUCs using only reproducible features overlapped with the CIs of CV-AUCs using all features. Therefore, using only reproducible features does not affect discriminative power. In clinical practice and multicenter studies,

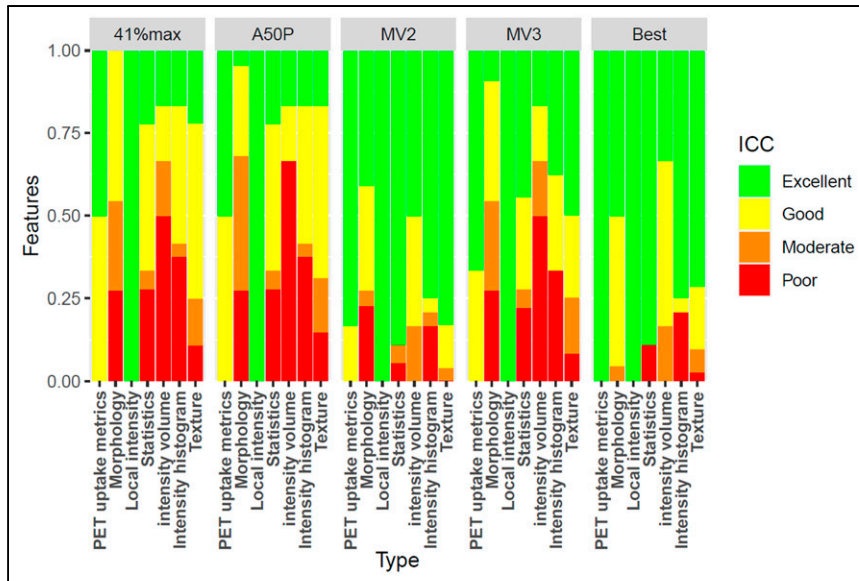


**FIGURE 3.** Percentage of radiomics features yielding excellent, good, moderate, or poor ICC agreement between SUV4.0 segmentation and the other methods for the largest lesion. 41%max = 41% of SUV<sub>max</sub>; A50P = 50% of SUV<sub>peak</sub>; MV2 = majority vote segmenting voxels detected by  $\geq 2$  methods; MV3 = majority vote segmenting voxels detected by  $\geq 3$  methods.

**TABLE 4**

Number of Independent Features per Segmentation Method, Number of Included Features, and Predictive Value for Largest Lesion for All Extracted Features ( $n = 483$ ) and All Reliable, Repeatable, and Reproducible Features ( $n = 99$ )

No. of features	Parameter	Independent of MTV	Independent of SUV <sub>peak</sub>	Independent of MTV and SUV <sub>peak</sub>	Independent of MTV and SUV <sub>peak</sub> and uncorrelated	No. of features in linear regression	CV-AUC ( $\pm$ SD)
483	SUV4.0	427	134	85	24	11	0.73 $\pm$ 0.10
	41%max	409	158	84	19	10	0.71 $\pm$ 0.11
	A50P	424	176	117	21	8	0.71 $\pm$ 0.11
	MV2	435	141	93	21	3	0.71 $\pm$ 0.10
	MV3	424	173	114	21	5	0.69 $\pm$ 0.11
	Best	437	168	122	25	10	0.69 $\pm$ 0.11
99	SUV4.0	57	46	13	10	5	0.73 $\pm$ 0.10
	41%max	50	57	14	6	1	0.65 $\pm$ 0.11
	A50P	54	59	20	9	4	0.63 $\pm$ 0.11
	MV2	59	52	18	8	3	0.70 $\pm$ 0.11
	MV3	54	52	18	7	3	0.67 $\pm$ 0.11
	Best	59	55	21	10	3	0.69 $\pm$ 0.11

41%max = 41% of SUV<sub>max</sub>; A50P = 50% of SUV<sub>peak</sub>; MV2 = majority vote segmenting voxels detected by  $\geq 2$  methods; MV3 = majority vote segmenting voxels detected by  $\geq 3$  methods.

variable image qualities are encountered. Therefore, some features that have high predictive values may in reality be difficult to measure reliably. It is thus advisable to only use reproducible features, especially in multicenter settings.

To our knowledge, this was the first study that assessed the influence of segmentation methods on PET radiomics features and their predictive power, other than MTV, in DLBCL. By applying multiple frequently used methods on the same patients, we could directly compare the effect of segmentation methods on quantitative PET radiomics features. We chose to calculate linear relations among radiomics features using Pearson correlation because we used logistic regression as a classifier, and the logistic regression model calculates linear relations with included features. This probably led to fewer included features in the logistic regression model compared with the application of Spearman correlation as data reduction method. One of the limitations of this study was that not all scans were scanned according to the EARL protocol; this inconsistency might affect the discriminative power and repeatability of features (25). Because we matched events and non-events on reconstruction method there were no difference in EARL compliance between groups. However, this matching does not preclude an effect of the reconstruction method on the discriminative power. Use of harmonization methods such as ComBat to retrospectively increase uniformity in large datasets has definitely been shown to be worthwhile (33,34). Therefore, ComBat-based data alignment would be a successful approach toward harmonizing these differences. Unfortunately, in our study the number of patients per center was too small to allow application of ComBat. Moreover, in view of the equivalent discriminative power seen in our data among various segmentation methods, ComBat-based data alignment would be a successful approach toward harmonizing databases of radiomics features analyzed using different segmentation methods. In our cohort, patients presented with high

MTVs; therefore, these results need to be validated for other cohorts with smaller lesion sizes.

**CONCLUSION**

This study found no substantial difference in the discriminative performance of radiomics features extracted using different segmentation methods. However, there are differences in the actual radiomics feature values derived and in the selected features among segmentation methods. Until consensus on a segmentation method for DLBCL is reached, it is advisable to use only prediction models that are built using data with the same segmentation methods.

**DISCLOSURE**

This work was financially supported by the Dutch Cancer Society (VU-2018-11648) and partially by the research program STRaTeGy (14929), which is financed by The Netherlands Organization for Scientific Research. No other potential conflict of interest relevant to this article was reported.

**KEY POINTS**

**QUESTION:** What is the influence of segmentation methods on the discriminative power of baseline radiomics features in DLBCL?

**PERTINENT FINDINGS:** There is no difference in the discriminative power of radiomics features among segmentation methods. However, different features are selected when applying different segmentation methods.

**IMPLICATIONS FOR PATIENT CARE:** It is advisable to only use prediction models that are build using data with the same segmentation methods.

## REFERENCES

- Crump M, Neelapu SS, Farooq U, et al. Outcomes in refractory diffuse large B-cell lymphoma: results from the international SCHOLAR-1 study. *Blood*. 2017;130:1800–1808.
- Cottreau AS, Nioche C, Dirand AS, et al. <sup>18</sup>F-FDG PET dissemination features in diffuse large B-cell lymphoma are predictive of outcome. *J Nucl Med*. 2020;61:40–45.
- Aide N, Fruchart C, Nganoa C, Gac AC, Lasnon C. Baseline <sup>18</sup>F-FDG PET radiomic features as predictors of 2-year event-free survival in diffuse large B cell lymphomas treated with immunochemotherapy. *Eur Radiol*. 2020;30:4623–4632.
- Ceriani L, Gritti G, Cascione L, et al. SAKK38/07 study: integration of baseline metabolic heterogeneity and metabolic tumor volume in DLBCL prognostic model. *Blood Adv*. 2020;4:1082–1092.
- International Non-Hodgkin's Lymphoma Prognostic Factors Project. A predictive model for aggressive non-Hodgkin's lymphoma. *N Engl J Med*. 1993;329:987–994.
- Ilyas H, Mikhaeel NG, Dunn JT, et al. Defining the optimal method for measuring baseline metabolic tumour volume in diffuse large B cell lymphoma. *Eur J Nucl Med Mol Imaging*. 2018;45:1142–1154.
- Barrington SF, Zwezerijnen BG, de Vet HC, et al. Automated segmentation of baseline metabolic total tumor burden in diffuse large B-cell lymphoma: which method is most successful? *J Nucl Med*. 2021;62:332–337.
- Senjo H, Hirata K, Izumiyama K, et al. High metabolic heterogeneity on baseline <sup>18</sup>F-FDG-PET/CT scan as a poor prognostic factor for newly diagnosed diffuse large B-cell lymphoma. *Blood Adv*. 2020;4:2286–2296.
- Eertink JJ, van de Brug T, Wiegers SE, et al. <sup>18</sup>F-FDG PET/CT baseline radiomics features are predictive of outcome in diffuse large B-cell lymphoma patients. *Eur J Nucl Med Mol Imaging*. August 18, 2021 [Epub ahead of print].
- Orlhac F, Soussan M, Maisonneuve JA, Garcia CA, Vanderlinden B, Buvat I. Tumor texture analysis in <sup>18</sup>F-FDG PET: relationships between texture parameters, histogram indices, standardized uptake values, metabolic volumes, and total lesion glycolysis. *J Nucl Med*. 2014;55:414–422.
- Tolosi L, Lengauer T. Classification with correlated features: unreliability of feature ranking and solutions. *Bioinformatics*. 2011;27:1986–1994.
- Zwanenburg A. Radiomics in nuclear medicine: robustness, reproducibility, standardization, and how to avoid data analysis traps and replication crisis. *Eur J Nucl Med Mol Imaging*. 2019;46:2638–2655.
- Kumar V, Gu Y, Basu S, et al. Radiomics: the process and the challenges. *Magn Reson Imaging*. 2012;30:1234–1248.
- Boellaard R, Delgado-Bolton R, Oyen WJ, et al. FDG PET/CT: EANM procedure guidelines for tumour imaging: version 2.0. *Eur J Nucl Med Mol Imaging*. 2015;42:328–354.
- Lugtenburg PJ, de Nully Brown P, van der Holt B, et al. Rituximab-CHOP with early rituximab intensification for diffuse large B-cell lymphoma: a randomized phase III trial of the HOVON and the Nordic Lymphoma Group (HOVON-84). *J Clin Oncol*. 2020;38:3377–3387.
- Boellaard R. Quantitative oncology molecular analysis suite: ACCURATE [abstract]. *J Nucl Med*. 2018;59(suppl 1):1753.
- Frings V, van Velden FH, Velasquez LM, et al. Repeatability of metabolically active tumor volume measurements with FDG PET/CT in advanced gastrointestinal malignancies: a multicenter study. *Radiology*. 2014;273:539–548.
- Burggraaff CN, Rahman F, Kassner I, et al. Optimizing workflows for fast and reliable metabolic tumor volume measurements in diffuse large B cell lymphoma. *Mol Imaging Biol*. 2020;22:1102–1110.
- Pfahler E, Zwanenburg A, de Jong JR, Boellaard R. RaCaT: an open source and easy to use radiomics calculator tool. *PLoS One*. 2019;14:e0212223.
- Zwanenburg A, Vallieres M, Abdalah MA, et al. The Image Biomarker Standardization Initiative: standardized quantitative radiomics for high-throughput image-based phenotyping. *Radiology*. 2020;295:328–338.
- Koo TK, Li MY. A guideline of selecting and reporting intraclass correlation coefficients for reliability research. *J Chiropr Med*. 2016;15:155–163.
- Mukaka MM. Statistics corner: a guide to appropriate use of correlation coefficient in medical research. *Malawi Med J*. 2012;24:69–71.
- Akaike H. Information theory and an extension of the maximum likelihood principle. In: Parzen E, Tanabe K, Kitagawa G, eds. *Selected Papers of Hirotugu Akaike*. Springer; 1998:199–213.
- Dietterich TG. Approximate statistical tests for comparing supervised classification learning algorithms. *Neural Comput*. 1998;10:1895–1923.
- Pfahler E, van Sluis J, Merema BBJ, et al. Experimental multicenter and multivendor evaluation of the performance of PET radiomic features using 3-dimensionally printed phantom inserts. *J Nucl Med*. 2020;61:469–476.
- Hatt M, Majdoub M, Vallieres M, et al. <sup>18</sup>F-FDG PET uptake characterization through texture analysis: investigating the complementary nature of heterogeneity and functional tumor volume in a multi-cancer site patient cohort. *J Nucl Med*. 2015;56:38–44.
- Brooks FJ, Grigsby PW. The effect of small tumor volumes on studies of intratumoral heterogeneity of tracer uptake. *J Nucl Med*. 2014;55:37–42.
- Hatt M, Tixier F, Cheze Le Rest C, Pradier O, Visvikis D. Robustness of intratumour <sup>18</sup>F-FDG PET uptake heterogeneity quantification for therapy response prediction in oesophageal carcinoma. *Eur J Nucl Med Mol Imaging*. 2013;40:1662–1671.
- Belli ML, Mori M, Broggi S, et al. Quantifying the robustness of [<sup>18</sup>F]FDG-PET/CT radiomic features with respect to tumor delineation in head and neck and pancreatic cancer patients. *Phys Med*. 2018;49:105–111.
- Cysouw MCF, Jansen BHE, van de Brug T, et al. Machine learning-based analysis of [<sup>18</sup>F]DCFPyL PET radiomics for risk stratification in primary prostate cancer. *Eur J Nucl Med Mol Imaging*. 2021;48:340–349.
- Altazi BA, Zhang GG, Fernandez DC, et al. Reproducibility of F18-FDG PET radiomic features for different cervical tumor segmentation methods, gray-level discretization, and reconstruction algorithms. *J Appl Clin Med Phys*. 2017;18:32–48.
- Bashir U, Azad G, Siddique MM, et al. The effects of segmentation algorithms on the measurement of <sup>18</sup>F-FDG PET texture parameters in non-small cell lung cancer. *EJNMMI Res*. 2017;7:60.
- Orlhac F, Boughdad S, Philippe C, et al. A postreconstruction harmonization method for multicenter radiomic studies in PET. *J Nucl Med*. 2018;59:1321–1328.
- Dissaux G, Visvikis D, Da-Ano R, et al. Pretreatment <sup>18</sup>F-FDG PET/CT radiomics predict local recurrence in patients treated with stereotactic body radiotherapy for early-stage non-small cell lung cancer: a multicentric study. *J Nucl Med*. 2020;61:814–820.